



RESEARCH ARTICLE

Raman response of topologically protected surface states in sub-micrometric $\text{Pb}_{0.77}\text{Sn}_{0.23}\text{Se}$ flakes

Sanaz Mehdipour¹ | David López-Díaz^{1,6} | María Mercedes Velázquez¹ | Pedro Hidalgo² | Bianchi Méndez² | Mónica Luna³ | Vittorio Bellani⁴ | Mario Amado¹ | Geetha Balakrishnan⁵ | Enrique Diez¹

¹Group of Nanotechnology, USAL-NANOLAB, University of Salamanca, Salamanca, 37008, Spain

²Departamento de Física de Materiales, Universidad Complutense de Madrid, Madrid, 28040, Spain

³Instituto de Micro y Nanotecnología (IMN-CNM-CSIC), Tres Cantos, Madrid, 28760, Spain

⁴Physics Department and INFN, University of Pavia, Pavia, 27100, Italy

⁵Department of Physics, University of Warwick, Coventry, CV4 7AL, UK

⁶Departamento de Química Analítica, Química Física e Ingeniería Química, University of Alcalá, Madrid, Madrid, 28871, Spain

Correspondence

Enrique Diez, Group of Nanotechnology, USAL-NANOLAB, University of Salamanca, 37008 Salamanca, Spain.
Email: enrisa@usal.es

Funding information

MINECO, Grant/Award Numbers:
MAT2016-75955, PID2019-106820RB-C22;
INFN CSNS/WIRES; EPSRC, UK, Grant/
Award Number: EP/T005963/; JCyL,
Grant/Award Number: SA256P18; EU
FEDER; JCyL (PhD fellowship grant);
ERDF and Junta de Castilla y León;
MCIU-AEI-FEDER-UE, Grant/Award
Number: RTI2018-096937-B-C22;
Comunidad de Madrid, Grant/Award
Number: P2018/EMT-4308

Abstract

The Raman spectra of the topological crystalline insulator $\text{Pb}_{0.77}\text{Sn}_{0.23}\text{Se}$ flakes of thickness below 150 nm show the presence of plasma enhanced phonons related to topologically protected surface electronic states. The Fröhlich interaction between the topologically protected surface Dirac electrons and the phonons activates the forbidden phonons near the center of the Brillouin zone. An overtone is observed at a higher wavenumber, with a resonant response with temperature, related to an enhancement of the long-range coupling between the topologically protected surface electrons and phonons.

KEY WORDS

Fröhlich interaction, phonon renormalization, plasma-enhanced phonons, topological crystalline insulators

1 | INTRODUCTION

Topological crystalline insulators (TCIs) represent a different class of topological insulator (TI) materials where crystalline symmetry replaces the role of time-reversal symmetry in TIs, ensuring topological protection and leading to the emergence of new important basic phenomena. Raman spectroscopy provides a contact-free technique to study the behavior of topological properties of materials with changing temperature. The temperature-dependent study of the Raman spectra on TI and TCI nanoflakes gives access to the information on the anharmonic phonon–phonon arising from the bulk material as well as the electron–phonon interaction that originate from the enhanced surface contribution. The temperature-dependent Raman spectra evidences the fact that Dirac fermions contribute significantly to the electron–phonon coupling, which manifests itself as a strong phonon renormalization in the topological materials at sufficiently low temperatures.^[1] Moreover, the discovery of graphene^[2] has aroused the growing interest in other layered materials,^[3,4] fostering radical developments in the field of nanotechnology. One of these not fully explored layered materials is $\text{Pb}_{1-x}\text{Sn}_x\text{Se}$ that is indeed a narrow gap semiconductor that, for Sn fraction of $x = 0.23$, behaves like a TCI.^[5] Although standard TIs are incidentally band insulators with a bulk energy gap and gapless boundaries that carry spin currents (i.e., edges in 2D or surfaces in 3D) protected by time-reversal symmetry,^[6–8] multiple surface states protected by crystalline symmetry (mirror symmetry) are present in TCIs.^[9,10] Very thin layers of the TI material will lead to an interplay between 2D effects and TI phenomena. Moreover, the thickness reduction leads to improve the carrier contribution from the topological surface states and minimize the bulk carrier densities.^[11] In this regard, new physics has been appearing in very thin layers of TIs;^[11] in particular, it has been found that, in very thin Bi_2Se_3 , the Dirac fermions contribute to the electron–phonon interactions, with a consequent strong phonon renormalization below a specific temperature (~ 120 K). Aimed at this finding, we have studied such behavior in a TCI, and our results indicate that the phenomena is present. We also find another evidence of the interaction between phonon and surface electrons: a mode at high energy ($\sim 300 \text{ cm}^{-1}$) due to the overtone of forbidden phonons very close to the center of the Brillouin zone, which are activated by the Fröhlich coupling.

Angle-resolved photoemission spectroscopy (ARPES) and scanning tunneling microscopy (STM) studies on surface states in TIs revealed that if the surface states are spin-independent, they will be immune from back-scattering and localization thereupon.^[12–16] As a

consequence, the main scattering mechanism is defined by electron–phonon interactions for surface Dirac fermions at finite temperatures.^[12] The electron–phonon interactions impact on the dispersion and lifetime of both the electronic and phonon states in a material.^[12] In this regard, the first principle calculations^[17] theoretically as well as the ARPES^[5] and the STM^[18] experiments confirmed the presence of topological surface states in $\text{Pb}_{1-x}\text{Sn}_x\text{Se}$ ($0 < x < 0.4$).

The discrimination between the surface and bulk-like behavior of the material leads to the emergence of fundamental phenomena. Indeed, in the case of bulk carrier densities (typical for semiconductors and insulators), all surface-related effects are masked by the bulk properties and anharmonic phonon–phonon interactions is the dominant scattering mechanism. Although in the case of electronic surface contributions, the electron–phonon coupling plays the crucial role. Moreover, the high-enough surface contribution brings about the phonon renormalization.^[1] In addition, these mechanisms have a temperature-dependent behavior, because at lower temperatures, phonons are frozen out and scattering mechanism is dominated by the electron–phonon coupling.^[1] Therefore, to investigate the contribution of Dirac fermions to the electron–phonon interaction which manifests itself in the strong phonon renormalization,^[1] we have performed a temperature-dependent Raman spectroscopy on thin films of $\text{Pb}_{0.77}\text{Sn}_{0.23}\text{Se}$. Because, it is a unique technique to study phononic and electronic properties of solids simultaneously.

The main motivation behind this study is to explore the presence of the topologically protected surface states in thin flakes of $\text{Pb}_{0.77}\text{Sn}_{0.23}\text{Se}$ by micro-Raman spectroscopy, where the surface states can be enhanced in comparison with the bulk ones. In fact, the profound appreciation of phonons and electron–phonon interactions in TCIs is of considerable importance to the pilot studies of topological transistors. Moreover, the observation of the Dirac-like linear band dispersion in band structures of TI surface states similar to the one in graphene^[19–21] triggered us to launch a systematic investigation on the Raman spectra of 3D bulk to 2D atomically thin samples of $\text{Pb}_{0.77}\text{Sn}_{0.23}\text{Se}$ as a function of sample thickness and temperature similar to those performed in other 2D materials.^[4,22–24]

2 | EXPERIMENTAL DETAILS

The $\text{Pb}_{0.77}\text{Sn}_{0.23}\text{Se}$ single crystals^[25] used in this study were grown by means of a modified Bridgman method where crystal boules of $\text{Pb}_{0.77}\text{Sn}_{0.23}\text{Se}$ were

produced following the procedure described by Tanaka et al.^[26] Initially, Pb-Sn-Se boules were synthesized from stoichiometric quantities of high-purity Pb and Sn shots (Alpha Aesar 99.99%) and powders of Sn and Se (Alpha Aesar 99.99%).^[25]

Indeed, $\text{Pb}_{1-x}\text{Sn}_x\text{Se}$ with $0 < x < 0.4$ has a rock salt crystal structure with a bandgap ($E_g \leq 0.29$ eV). PbSe and SnSe are two precursors of $\text{Pb}_{1-x}\text{Sn}_x\text{Se}$. Although PbSe is a topological trivial insulator with rock salt structure and direct bandgap of ~ 0.28 eV, SnSe is a trivial insulator with an orthorhombic structure and large bandgap of ~ 0.9 eV.^[27]

In this study, the $\text{Pb}_{0.77}\text{Sn}_{0.23}\text{Se}$ thin flakes were prepared by conventional mechanical exfoliation technique^[28] using scotch tape directly from the $\text{Pb}_{0.77}\text{Sn}_{0.23}\text{Se}$ bulk material along the edge of (001) plane and transferred to thermally oxidized Si substrate covered with 290-nm-thick SiO_2 layer shortly afterwards. The thickness of the resultant flakes varies around from 15 to 225 nm.

Raman scattering spectroscopy was carried out using micro-Raman spectrometer (LabRAM from Horiba Jobin-Yvon) in the backscattering configuration

excited with a solid-state red laser ($\lambda = 632.8$ nm). The light power at the laser exit was below 4 mW and linearly polarized. The temperature-dependent Raman measurements were carried out with the samples placed in a Janis ST-500 microscopy cryostat, spanning from 80 K to room temperature. The backscattered signal was collected through a log focal objective LMPlanfl Olympus 50 \times (NA = 0.5; working distance = 10.6 mm) resulting in a laser spot area on the sample of 5 μm . The scattered light was collected by a silicon CCD detector, with integration time of 30 s. Moreover, the same measurements were performed on different flakes with similar thickness to ensure the reliability of the measurements. The thickness of the different $\text{Pb}_{0.77}\text{Sn}_{0.23}\text{Se}$ flakes was measured by atomic force microscopy (AFM) technique, in a Nanotech AFM instrument controlled by Dulcinea system.^[29] The AFM mappings are very helpful to understand the resultant Raman data as a function of the flakes' thicknesses. The AFM topography images have been analyzed by a linear fitting of the top surface of the flakes and the corresponding substrate surface. Figure 1c–e shows the AFM profiles of some

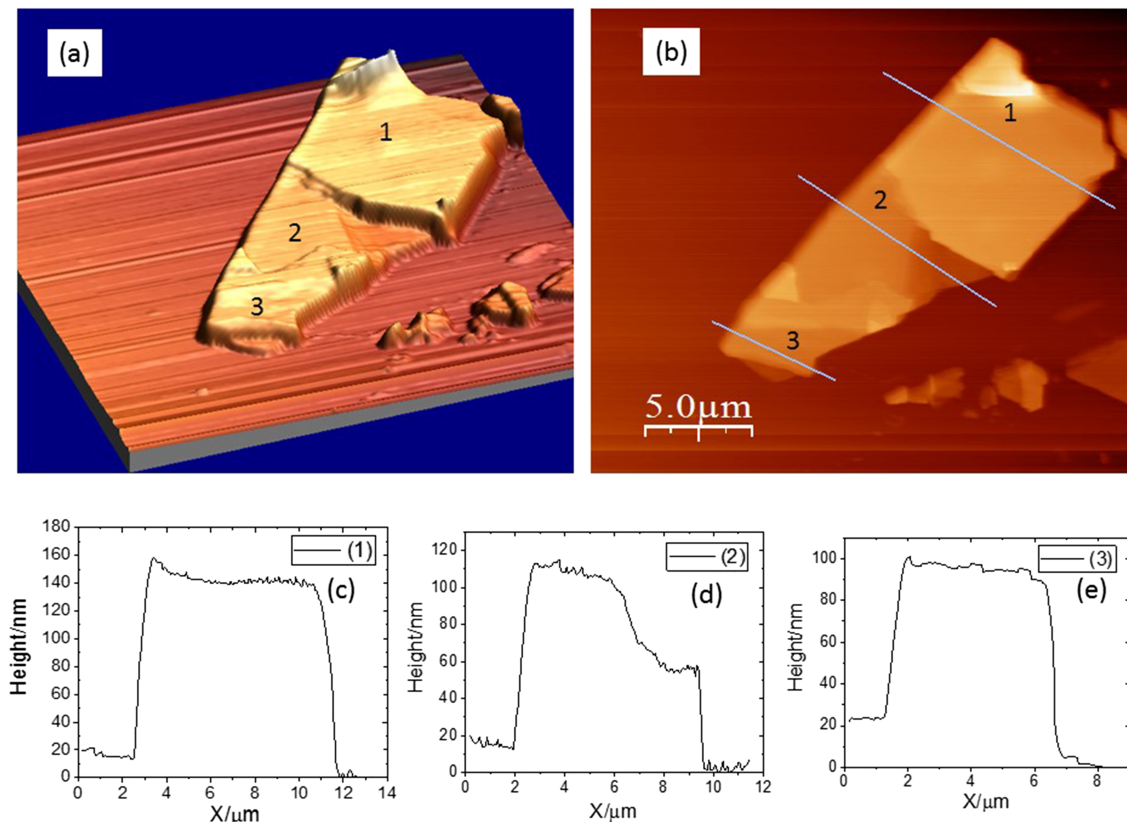


FIGURE 1 (a) 3D and (b) 2D atomic force microscopy images of thin flakes of exfoliated $\text{Pb}_{0.77}\text{Sn}_{0.23}\text{Se}$ with several areas with different thicknesses. We also show (c–e) the profile across three terraces along the lines showed in (b) and labeled as (c) 1, (d) 2, and (e) 3 [Colour figure can be viewed at wileyonlinelibrary.com]

$\text{Pb}_{0.77}\text{Sn}_{0.23}\text{Se}$ terraces using the WSxM software that will be characterized by Raman spectroscopy in the next section.

3 | RESULTS AND DISCUSSION

3.1 | Room-temperature Raman spectra of $\text{Pb}_{0.77}\text{Sn}_{0.23}\text{Se}$

The Raman measurements on different flakes of $\text{Pb}_{0.77}\text{Sn}_{0.23}\text{Se}$ reveal that depending on the thickness of the different terraces, different Raman bands are present. Figure 2 shows that for flakes with thickness below 3 μm , several Raman peaks are observed, among them the ones at 111 cm^{-1} , 154 cm^{-1} , 184 cm^{-1} , and 250 cm^{-1} (see Figure 2). These modes have been identified following the work of Ovsyannikov et al.^[30] which focused on the identification of the Raman modes in lead chalcogenides, comparing literature on experimental and theoretical results. The peak at 130 cm^{-1} in the freshly cleaved bulk is the longitudinal optical (LO) mode.^[30–32] We can see that the plasma-enhanced phonon (PEP) appears in the samples with thicknesses of 100–140 nm, which we ascribe the LO, shifted to high energy and plasma-enhanced. Indeed, Raman measurements of Glinka et al.^[33] on thin-films of the TI Bi_2Se_3 also revealed phonon energy renormalization and nonmonotonic enhancement of the electron-phonon coupling strength. The enhancement of the phonon response that we now observe in our TCI $\text{Pb}_{0.77}\text{Sn}_{0.23}\text{Se}$ thin flakes is possibly also due to the plasmon-phonon coupling which strengthens the electron-phonon interaction when the

free carrier density in Dirac surface states increases, with reducing the flake thickness. We can note that at Position 1, the PEP is shifted by $\sim 3\text{ cm}^{-1}$ at higher wavenumber than at Positions 2 and 3. We repeated the measurement several times, finding that it is not an experimental artifact. We think that this shift is because the renormalization of phonon energies for the metal-type 2D Dirac surface states is very sensitive to the local structural and electronic properties of the flake.^[1,34] Rocksalt crystals have 3D (T or F) phonons and generate Raman active (A) and 2D (E) phonons. We did not observe these modes; if present, they are below the detection limits.

3.2 | Temperature-dependent Raman spectra of $\text{Pb}_{0.77}\text{Sn}_{0.23}\text{Se}$

We measured the Raman spectra in the thin flakes, as a function of temperature, in order to explore the interplay between phonons and topologically protected surface states. Recent Raman measurements on TI nanoflakes show that the temperature dependency of the phonon dynamics in TI is simultaneously driven by anharmonic phonon-phonon interaction from bulk behavior and contributions from the electron-phonon interaction originating from the enhanced surface contribution. The Dirac fermions contribute significantly to the electron-phonon coupling, which manifests itself in strong phonon renormalizations in the TI at temperatures below a specific temperature.^[1] In case of $\text{Pb}_{0.77}\text{Sn}_{0.23}\text{Se}$ due to its temperature-dependent band inversion, at low temperature, an interplay between anharmonicity, electron-phonon coupling, and topology takes place. It is expected

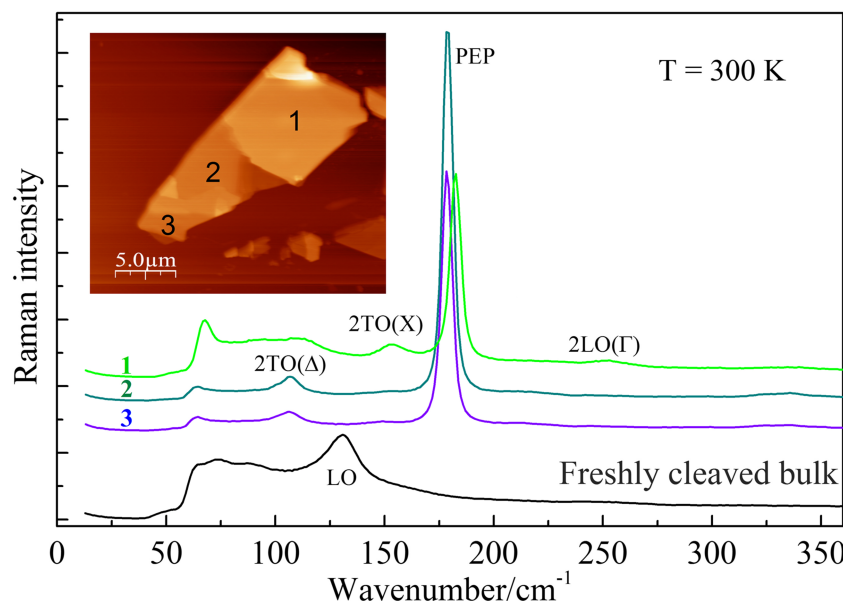


FIGURE 2 The comparison between the Raman bands of $\text{Pb}_{0.77}\text{Sn}_{0.23}\text{Se}$ thin flakes and a freshly cleaved bulk sample. The thicknesses of areas with Labels 1, 2, and 3 are 140 nm, 110 nm, and 95 nm, respectively. The spectra have been vertically shifted for clarity [Colour figure can be viewed at wileyonlinelibrary.com]

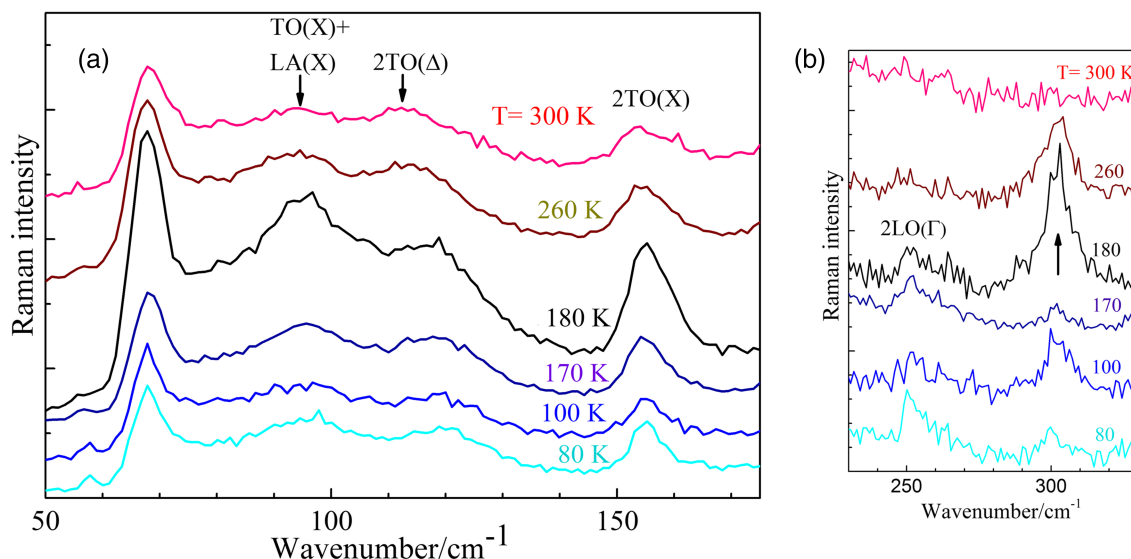


FIGURE 3 The Raman spectra as a function of temperature measured on Area 1 (see Figure 1) (a) below and (b) above 200 cm^{-1} . The spectra have been vertically shifted and arrows added determining the position of some of the peaks for clarity [Colour figure can be viewed at wileyonlinelibrary.com]

that $\text{Pb}_{1-x}\text{Sn}_x\text{Se}$ ($x = 0.23$) as a TCI material has Dirac-like surface states that cross the bandgap. To observe this phenomenon, there must be a transition from a normal state (trivial insulator) to an inverted bandgap state (nontrivial TCI state).^[4] There are some ways to accomplish this transition, namely by varying the composition of the solid solution x ,^[30] or by changing the temperature T ,^[4,35,36] or by applying hydrostatic pressure.^[4,37] Moreover, the ARPES studies on the (001) surface of $\text{Pb}_{0.77}\text{Sn}_{0.23}\text{Se}$ and $\text{Pb}_{0.70}\text{Sn}_{0.30}\text{Se}$ ^[38] monocrystals revealed that the topological nature and the surface-state electronic structure in this material are sensitive to temperature. Indeed, the thermodynamic expansion of the lattice constant accounts for the thermodynamic evolution of the surface-state electronic structure for the transition from the trivial phase to the TCI phase.^[38] In other words, for the temperatures higher than 100 K, there is a gap between the surface states (trivial phase). As the temperature goes down, the gapped surface states start approaching the X-shaped ones similar to Dirac fermion states (nontrivial TCI phase). In Figure 3, the temperature-dependent Raman measurement of a layer of $\text{Pb}_{0.77}\text{Sn}_{0.23}\text{Se}$ with 140-nm thickness (Region 1 in Figure 2) has been recorded in the 80 K–300 K temperature range to know more about the dynamics of its crystal lattice by analyzing the temperature-dependent behavior of its modes. We calculated the temperature coefficient of the observed modes, finding the following values: $-0.099\text{ cm}^{-1}\text{ K}^{-1}$ for $\text{TO}(X) + \text{LA}(X)$, $-0.036\text{ cm}^{-1}\text{ K}^{-1}$ for $2\text{TO}(\Delta)$, and $-0.009\text{ cm}^{-1}\text{ K}^{-1}$ for $2\text{TO}(X)$, which are comparable with the estimated values of other 2D materials such as MoS_2 and WS_2MoSe_2 . The calculated temperature coefficient of

peak positions in comparison with other 2D materials are tabulated in the supplementary material. At temperature around 180 K, a mode close to 300 cm^{-1} appears (which is marked with an arrow), related to an enhancement of the long-range coupling between the topologically protected surface electrons and phonons. We attribute this mode to the first overtone of the LO phonon (2LO) close to the center of the Brillouin zone explained by Fröhlich resonance mechanism. Another signature of the Fröhlich interaction is that with increasing temperature, its contribution to the 2LO scattering decreases due to the erosion of the resonance.^[39] As depicted in Figure 3, there is a surge in the $2\text{TO}(X)$ mode around the temperature of 180 K.

4 | CONCLUSIONS

In this work, the Raman spectroscopy studies of exfoliated $\text{Pb}_{0.77}\text{Sn}_{0.23}\text{Se}$ thin flakes have been carried out. The obtained results have demonstrated that there is a thickness dependency on the Raman data of this material. In the case of thin flakes with thicknesses below 150 nm, the presence of plasma-enhanced phonons related to topologically protected surface electronic states by the appearance of a peak around 184 cm^{-1} is confirmed. At a temperature of 180 K, the Fröhlich interaction between the phonons and the topologically protected surface Dirac electrons activates the forbidden single LO phonon near the center of the Brillouin zone. We have observed its 2LO overtone at higher wavenumber, and with increasing the temperature, the Fröhlich contribution to the 2LO scattering decreases due to the erosion of the resonance.

ACKNOWLEDGEMENTS

We thank Juan Antonio Delgado Notario and María Pilar Castroviejo for their assistance with the Raman measurements at Salamanca and Burgos. This work has been supported by the following grants: MINECO MAT2016-75955 and PID2019-106820RB-C22, INFN CSN5/WIRES, EPSRC, UK EP/T005963/, JCYL SA256P18, and EU FEDER funds. S. M. thanks JCyL (PhD fellowship grant), D. L. L. thanks ERDF and Junta de Castilla y León for his postdoc contract, and M. L. acknowledges MCIU-AEI-FEDER-UE (RTI2018-096937-B-C22) and Comunidad de Madrid (P2018/EMT-4308).

ORCID

David López-Díaz  <https://orcid.org/0000-0002-6231-6233>

Maria Mercedes Velázquez  <https://orcid.org/0000-0003-2746-8204>

Geetha Balakrishnan  <https://orcid.org/0000-0002-5890-1149>

Enrique Diez  <https://orcid.org/0000-0001-7964-4148>

REFERENCES

- [1] S. Buchenau, S. Scheitz, A. Sethi, J. E. Slimak, T. E. Glier, P. K. Das, T. Dankwort, L. Akinsinde, L. Kienle, A. Rusydi, C. Ulrich, S. L. Cooper, M. Rübhausen, *Phys. Rev. B: Condens. Matter* **2020**, *101*, 245431.
- [2] K. S. Novoselov, A. K. Geim, S. V. Morozov, D. Jiang, Y. Zhang, S. V. Dubonos, I. V. Grigorieva, A. A. Firsov, *Science* **2004**, *306*, 666.
- [3] Q. H. Wang, K. Kalantar-Zadeh, A. Kis, J. N. Coleman, M. S. Strano, *Nat. Nanotechnol.* **2012**, *7*, 699.
- [4] A. S. Pawbake, M. S. Pawar, S. R. Jadkar, D. J. Late, *Nanoscale* **2016**, *8*, 3008.
- [5] P. Dziawa, B. J. Kowalski, K. Dybko, R. Buczko, A. Szczerbakow, M. Szot, E. Łusakowska, T. Balasubramanian, B. M. Wojek, M. H. Berntsen, O. Tjernberg, T. Story, *Nat. Mater.* **2012**, *11*, 1023.
- [6] M. Shuichi, *New J. Phys.* **2007**, *9*, 356.
- [7] M. Z. Hasan, C. L. Kane, *Rev. Mod. Phys.* **2010**, *82*, 3045.
- [8] X.-L. Qi, S.-C. Zhang, *Rev. Mod. Phys.* **2011**, *83*, 1057.
- [9] J. Shen, J. J. Cha, *Nanoscale* **2014**, *6*, 14133.
- [10] L. Fu, *Phys. Rev. Lett.* **2011**, *106*, 106802.
- [11] J. Liu, T. H. Hsieh, P. Wei, W. Duan, J. Moodera, L. Fu, *Nat. Mater.* **2014**, *13*, 178.
- [12] X. Zhu, L. Santos, C. Howard, R. Sankar, F. C. Chou, C. Chamon, M. El-Batanouny, *Phys. Rev. Lett.* **2012**, *108*, 185501.
- [13] P. Roushan, J. Seo, C. V. Parker, Y. S. Hor, D. Hsieh, D. Qian, A. Richardella, M. Z. Hasan, R. J. Cava, A. Yazdani, *Nature* **2009**, *460*, 1106.
- [14] T. Zhang, P. Cheng, X. Chen, J.-F. Jia, X. Ma, K. He, L. Wang, H. Zhang, X. Dai, Z. Fang, X. Xie, Q.-K. Xue, *Phys. Rev. Lett.* **2009**, *103*, 266803.
- [15] L. A. Wray, S.-Y. Xu, Y. Xia, D. Hsieh, A. V. Fedorov, Y. S. Hor, R. J. Cava, A. Bansil, H. Lin, M. Z. Hasan, *Nat. Phys.* **2011**, *7*, 32.
- [16] D. Hsieh, Y. Xia, D. Qian, L. Wray, J. H. Dil, F. Meier, J. Osterwalder, L. Patthey, J. G. Checkelsky, N. P. Ong, A. V. Fedorov, H. Lin, A. Bansil, D. Grauer, Y. S. Hor, R. J. Cava, M. Z. Hasan, *Nature* **2009**, *460*, 1101.
- [17] T. H. Hsieh, H. Lin, J. Liu, W. Duan, A. Bansil, L. Fu, *Nat. Commun.* **2012**, *3*, 982.
- [18] Y. Okada, M. Serbyn, H. Lin, D. Walkup, W. Zhou, C. Dhital, M. Neupane, S. Xu, Y. J. Wang, R. Sankar, F. Chou, A. Bansil, M. Z. Hasan, S. D. Wilson, L. Fu, V. Madhavan, *Science* **2013**, *341*, 1496.
- [19] M. S. Dresselhaus, A. Jorio, M. Hofmann, G. Dresselhaus, R. Saito, *Nano Lett.* **2010**, *10*, 751.
- [20] L. M. Malard, M. A. Pimenta, G. Dresselhaus, M. S. Dresselhaus, *Phys. Rep.* **2009**, *473*, 51.
- [21] A. H. Castro Neto, F. Guinea, N. M. R. Peres, K. S. Novoselov, A. K. Geim, *Rev. Mod. Phys.* **2009**, *81*, 109.
- [22] M. Paillet, R. Parret, J.-L. Sauvajol, P. Colomban, *J. Raman Spectrosc.* **2018**, *49*, 8.
- [23] T. C. V. Carvalho, F. D. V. Araujo, C. C. de Santos, L. M. R. Alencar, J. Ribeiro-Soares, D. J. Late, A. O. Lobo, A. G. S. Filho, R. S. Alencar, B. C. Viana, *AIP Adv* **2019**, *9*, 085316.
- [24] M. S. Pawar, D. J. Late, *Beilstein J. Nanotechnol.* **2019**, *10*, 467.
- [25] G. Balakrishnan, M. Saghir, M. R. Lees, S. J. York, S. A. Hindmarsh, A. M. Sanchez, M. Walker, C. F. McConville, *J. Indian Inst. Sci.* **2016**, *96*, 122.
- [26] Y. Tanaka, Z. Ren, T. Sato, K. Nakayama, S. Souma, T. Takahashi, K. Segawa, Y. Ando, *Nat. Phys.* **2012**, *8*, 800.
- [27] N. Anand, S. Buvaev, A. F. Hebard, D. B. Tanner, Z. Chen, Z. Li, K. Choudhary, S. B. Sinnott, G. Gu, C. Martin, *Phys. Rev. B: Condens. Matter* **2014**, *90*, 235143.
- [28] Y. Huang, E. Sutter, N. N. Shi, J. Zheng, T. Yang, D. Englund, H.-J. Gao, P. Sutter, *ACS Nano* **2015**, *9*, 10612.
- [29] I. Horcas, R. Fernández, J. M. Gómez-Rodríguez, J. Colchero, J. Gómez-Herrero, A. M. Baro, *Rev. Sci. Instrum.* **2007**, *78*, 013705.
- [30] S. V. Ovsyannikov, Y. S. Ponosov, V. V. Shchennikov, V. E. Mogilenskikh, *Phys. Status Solidi C* **2004**, *1*, 3110.
- [31] L. Vodop'yanov, I. Kucherenko, A. Shotov, R. Scherm, *J ETP Lett.* **1978**, 27.
- [32] L. K. Vodop'yanov, L. A. Fal'Kovskī, J. Irvin, S. Himenis, *Sov. J. Exp. Theor. Phys. Lett.* **1991**, *53*, 586.
- [33] Y. D. Glinka, S. Babakiray, D. Lederman, *J. Appl. Phys.* **2015**, *118*, 135713.
- [34] B. K. Ridley, *Quantum Processes in Semiconductors*; OUP Oxford, **1999**.
- [35] L. Ci, Z. Zhou, L. Song, X. Yan, D. Liu, H. Yuan, Y. Gao, J. Wang, L. Liu, W. Zhou, G. Wang, S. Xie, *Appl. Phys. Lett.* **2003**, *82*, 3098.
- [36] I. Calizo, A. A. Balandin, W. Bao, F. Miao, C. N. Lau, *Nano Lett.* **2007**, *7*, 2645.
- [37] C. Postmus, J. R. Ferraro, S. S. Mitra, *Phys. Rev.* **1968**, *174*, 983.
- [38] A. A. Reijnders, J. Hamilton, V. Britto, J.-B. Brubach, P. Roy, Q. D. Gibson, R. J. Cava, K. S. Burch, *Phys. Rev. B: Condens. Matter* **2014**, *90*, 235144.
- [39] M. Neupane, S.-Y. Xu, R. Sankar, Q. Gibson, Y. J. Wang, I. Belopolski, N. Alidoust, G. Bian, P. P. Shibayev, D. S. Sanchez,

Y. Ohtsubo, A. Taleb-Ibrahimi, S. Basak, W. F. Tsai, H. Lin, T. Durakiewicz, R. J. Cava, A. Bansil, F. C. Chou, M. Z. Hasan, *Phys. Rev. B: Condens. Matter* **2015**, 92, 075131.

SUPPORTING INFORMATION

Additional supporting information may be found online in the Supporting Information section at the end of this article.

How to cite this article: Mehdipour S, López-Díaz D, Velázquez MM, et al. Raman response of topologically protected surface states in sub-micrometric $\text{Pb}_{0.77}\text{Sn}_{0.23}\text{Se}$ flakes. *J Raman Spectrosc.* 2020;51:2489–2495. <https://doi.org/10.1002/jrs.5998>